

We are IntechOpen, the world's leading publisher of Open Access books Built by scientists, for scientists

6,900

Open access books available

186,000

International authors and editors

200M

Downloads

Our authors are among the

154

Countries delivered to

TOP 1%

most cited scientists

12.2%

Contributors from top 500 universities



WEB OF SCIENCE™

Selection of our books indexed in the Book Citation Index
in Web of Science™ Core Collection (BKCI)

Interested in publishing with us?
Contact book.department@intechopen.com

Numbers displayed above are based on latest data collected.
For more information visit www.intechopen.com



One-Step Holographic Photoalignment for Twisted Nematic Liquid Crystal Gratings

Kotaro Kawai, Moritsugu Sakamoto, Kohei Noda,
Tomoyuki Sasaki, Nobuhiro Kawatsuki and
Hiroshi Ono

Additional information is available at the end of the chapter

<http://dx.doi.org/10.5772/67293>

Abstract

Liquid crystal gratings, in which liquid crystal molecules are periodically aligned, are fabricated by highly efficient and practical one-step holographic photoalignment method using a photocrosslinkable polymer liquid crystal (PCLC). This method is an innovative fabrication technique for liquid crystal grating containing a twisted nematic alignment, which does not require a conventional complex fabrication process. In this chapter, three types of liquid crystal gratings with twisted nematic alignment are fabricated. Periodic director distributions of these liquid crystal gratings are analyzed based on the elastic continuum theory and observed experimentally using a polarized light optical microscope. Furthermore, the polarization diffraction properties were measured by illumination with a visible laser beam. The resultant liquid crystal gratings exhibit various polarization diffraction properties depending on the director distributions and the polarization states of the incident beams. These polarization diffraction properties are well explained by theoretical analysis based on Jones calculus. These resultant liquid crystal gratings exhibit great potential for application as a diffractive optical element that can simultaneously control the various parameters of the light wave, such as amplitude, polarization states, and propagation direction.

Keywords: diffraction gratings, liquid crystals, polarization, Jones calculus, photocrosslinkable polymer liquid crystals

1. Introduction

Control of the various parameters, such as amplitude, polarization states, wavelength, and propagation direction of the light wave, is of great importance in a wide range of fields,

including the optoelectronics field. In particular, diffractive optical elements, in which light wave propagation is controlled by diffraction phenomena, are expected to realize such a function. Generally, light propagating inside the diffractive optical element is diffracted by inducing a phase difference to the light propagating through a medium whose shape or isotropic refractive index is periodically modulated. In addition, anisotropic diffractive optical elements in which the optical anisotropy is periodically modulated have been reported [1–10]. Anisotropic diffractive optical elements show the polarization controllability which the diffraction efficiency and polarization states depend on the polarization states of the incident beams. This is because various modulations of an effective refractive index along a grating vector depend on incident electric field vectors.

Structures, fabrication techniques, and materials of anisotropic diffraction gratings are wide ranging. In particular, polarization holographic recordings on an azobenzene-containing material are a typical fabrication technique and materials [1]. When two orthogonally (i.e., the product of the electric field vector and the complex conjugate of the other electric field vectors is zero) polarized beams interfere with each other, the polarization state is periodically modulated in the interference field; however, the intensity is not modulated. Therefore, with simultaneously induced photoisomerization reactions depending on a direction of incident polarized light, a periodically modulated anisotropic structure is fabricated by exposure of azobenzene polymer films to the orthogonal polarization interference field. In addition, liquid crystal (LC) gratings, in which LC directors are periodically modulated by periodically aligned films, are mentioned as an example of anisotropic diffractive optical elements [2–10]. Photoalignment by holographic exposure [2, 4, 8, 9], photo-masking exposure [3], microrubbing method [5], and using an interdigitated electrode [6] are the common methods of the fabrication methods of LC gratings. Photoreactive polymer LCs are mentioned as materials to use for alignment films other than azobenzene-containing material [2–4, 7–10]. LC gratings can be applied to optical switching elements by applying a voltage [2, 4–6]. Moreover, control of diffraction properties and wavelength selection properties is realized by birefringence control in LC gratings using temperature control [10]. In addition, diffraction efficiencies of each diffraction order (i.e., the direction of propagation) can be controlled by the incident polarization in LC gratings in which the LC directors continuously rotate along the grating vector [2, 4, 7, 8]. LC grating is not limited to a transmission type; there is also a reflection type [4]. The diffraction efficiency of LC grating is higher than the anisotropic diffractive optical elements of thin film type. This is because the thickness of the structure LC grating induces a large phase difference due to a thick structure. Based on these, LC gratings are suitable to be applied to optical elements that can simultaneously control the parameters of a light wave. However, fabricating an LC grating requires periodically and finely alignment processing in two alignment films and accurate fabrication technique so as not to shift the two alignment patterns.

In this chapter, we propose the efficient yet practical method for fabricating LC gratings containing a twisted nematic (TN) alignment structure using polarization holographic photoalignment and photocrosslinkable polymer LC (PCLC) synthesized by us as alignment films. First, as a preliminary experiment, we experimentally demonstrate that different patterns between two alignment substrates can be applied by one-step linearly polarized UV beam irradiation to an empty glass cell whose inner walls are coated with PCLC films. In

In addition, we show that fabrication of three types of LC gratings by one-step exposure of the empty glass cells to polarized interference UV fields. The periodic director distributions of the resultant LC gratings are observed experimentally by polarized light microscopy and are analyzed based on the elastic continuum theory. Furthermore, the polarization diffraction properties are measured experimentally by the incident of a visible laser and analyzed theoretically by Jones calculus.

2. One-step photoalignment for fabricating a TN-LC cell

2.1. Materials

In this chapter, a PCLC with 4-(4-methoxycinnamoyloxy)biphenyl side groups (P6CB) is adopted as materials of alignment substrates. The chemical structure of P6CB is shown in **Figure 1**. The synthetic method and the details of the characteristics can be found in reference [11]. In the P6CB alignment films after linearly polarized UV light exposure, axis-selective cross-linked LC mesogens act as a trigger, the cooperative reorientation of the side chains is induced during the annealing process as shown in **Figure 2**. The LC mesogen alignment due to the cross-linking reaction is thermally and long-term stable. P6CB shows the absorption in the ultraviolet light; however, it does not show absorption in the visible region. Therefore, P6CB is suitable for application to optical elements. In addition, the order parameter of P6CB depends on cross-linking density, which is proportional to the exposure dose. When the exposure dose is greater than 100 mJ/cm², mesogens of P6CB are oriented parallel to the polarization direction of linearly polarized UV after the annealing process. However, when the exposure dose is less than 100 mJ/cm², mesogens are oriented perpendicularly to the polarization direction of the linearly polarized UV.

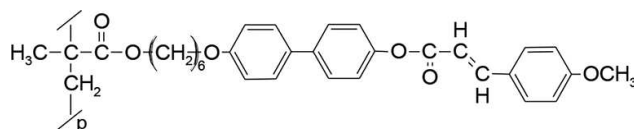


Figure 1. Chemical structure of PCLC with 4-(4-methoxycinnamoyloxy)biphenyl side groups (P6CB).

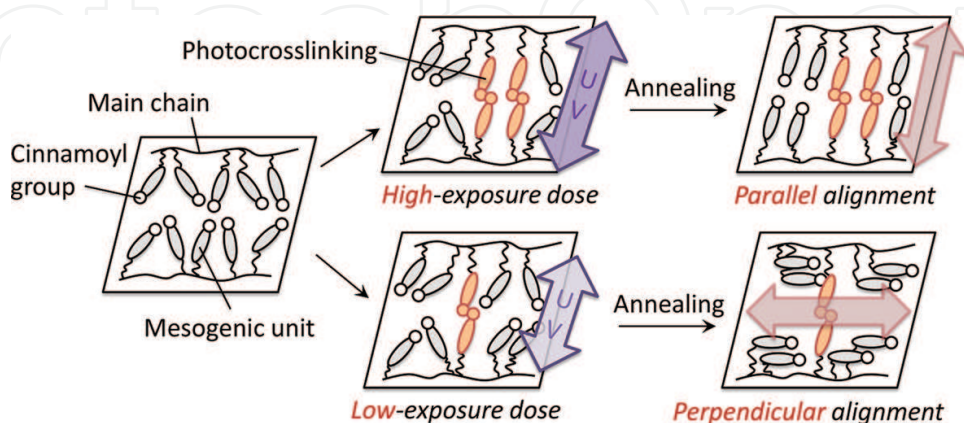


Figure 2. Schematic illustration of alignment mechanism and dependence of alignment direction on exposure dose in the P6CB.

2.2. Experiment and results

By applying the feature of P6CB described above, we propose a one-step photoalignment method as shown in **Figure 3**. In this one-step photoalignment method, orthogonal alignment direction between the two P6CB substrates is applied by linearly polarized UV beam irradiation to an empty glass cell whose inner walls are coated with P6CB. The one-step photoalignment method is realized by leveraging the phenomenon that the exposure dose between the two P6CB films is different due to the light absorption in the front P6CB film as shown in **Figure 3**. Therefore, a TN-aligned LC cell can be fabricated by injecting low-molecular-mass LCs in the empty glass cell. The experimental procedure and results of the demonstration experiment of the one-step photoalignment are described below.

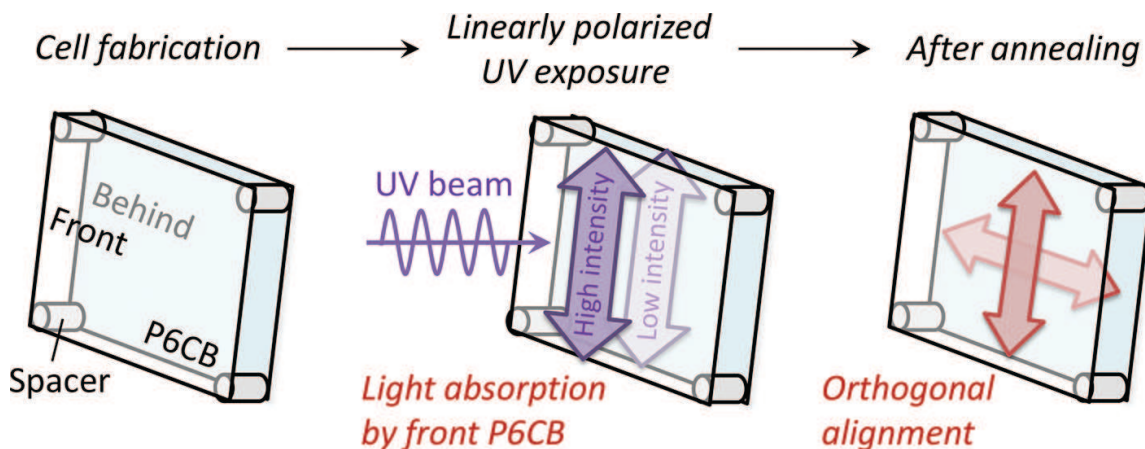


Figure 3. Schematic illustration of fabrication procedure of TN-LC cell by one-step photoalignment method.

P6CB substrates were prepared by spin coating, a solution of 1.5 wt% P6CB in methylene chloride on cleaned glass substrates. The spin coating in the first step is carried out for 3.0 s at 500 rpm, and then the second step is carried out for 40.0 s at 1500 rpm; these steps are continuous. The thickness of the resultant P6CB films on the glass substrates was 0.3 μm . An empty glass cell was fabricated by interposing 12 μm -thick spacers between two P6CB substrates, and then these were adhered using an epoxy-based adhesive. The empty glass cell was exposed to the linearly polarized UV beam as shown in **Figure 3**. A 325 nm wavelength He-Cd laser, which operates in TEM_{00} mode and emits a linear polarization, was used as the light source. The cross-sectional area of the beam was set to 0.04 cm^2 using two planoconvex lenses with different focal lengths. The beam intensity was set to 50 mW/cm^2 . In this experiment, the exposure dose varied from 90 to 525 mJ/cm^2 in 72.5 mJ/cm^2 steps by changing the exposure time from 1.8 to 10.5 s. After laser irradiation, the empty glass cell was annealed at 150°C for 15 min. After cooling to room temperature, the empty glass cell was filled with the nematic LC 4-pentyl-4'-cyanobiphenyl (5CB, Merck Japan K-15) through capillary action. The transmitted light from the resultant LC cell was observed by crossed Nichols method when a white light was used as the light source. In addition, the polarization state of the transmitted light was measured by the rotation-analyzer method using a Glan-Thompson prism as the analyzer. A 633 nm wavelength linearly polarized He-Ne laser, which was incident normal to the plane of the P6CB substrates, was used as the probe beam.

Figure 4 shows the photograph of the resultant LC cell under crossed Nicol polarizers and the polarization states of the incident and transmitted beams. The polarization direction of the irradiated linearly polarized UV beam in the photoalignment process is parallel to the transmission axis of the analyzer as shown in **Figure 4(a)**. Therefore, the bright fields and the dark fields are 90° TN alignment and 0° planar alignment, respectively. The 0° planar alignment structure can be also fabricated. This is because the sufficient exposure dose to align the P6CB along the polarization direction of the irradiated UV beam in the behind substrates can be given by increasing the exposure dose to the empty glass cell. The transmittance of the 325 nm wavelength UV beam in the front P6CB substrate is approximately 30%; however, the transmittance increases gradually during UV irradiation. The alignment structures are different between the inside and the outside of the exposed spots because the transverse mode of the irradiated UV laser is TEM₀₀ (i.e., an intensity distribution in accordance with a Gaussian function exists in the beam cross section). **Figure 4(b)** shows the polarization states of the incident and transmitted beams which through the spots are exposed at 235 mJ/cm² (TN, the third spot from the left) and 525 mJ/cm² (planar, the rightmost) in the photoalignment process. The polar plot represents the azimuthal distribution of the measured light intensity. The polarization azimuth of the probe beam which was transmitted through the TN alignment regions rotates 90°. Note that, the probe beam is not completely rotated 90° because the resultant LC cell does not strictly satisfy Morgan condition. Moreover, in the 0° planar alignment regions, the polarization states do not vary. These results indicate that the 90° TN and 0° planar alignment can be fabricated by one-step photoalignment method.

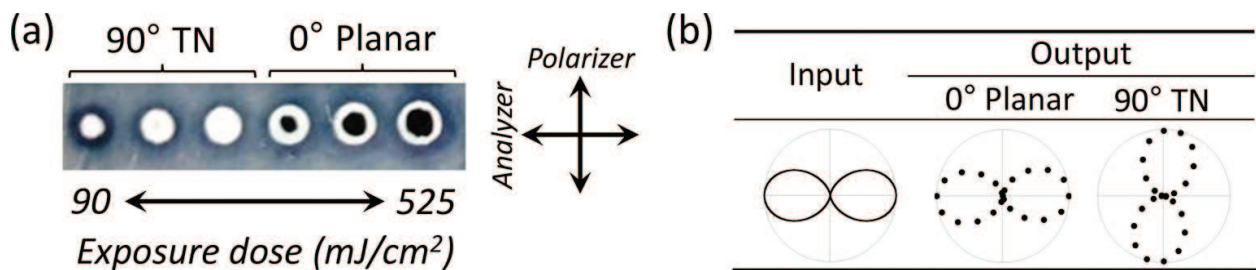


Figure 4. (a) Photograph of the resultant LC cell fabricated by one-step photoalignment under crossed Nicol polarizers. (b) Polarization states of the input and the output beams.

3. TN-LC gratings fabricated by one-step holographic photoalignment

3.1. Holographic photoalignment

LC gratings containing the TN alignment can be fabricated by extended to an interference exposure from the single beam one-step photoalignment described above. By exposure of the empty glass cell to UV interference beam in which polarization states are periodically modulated, LC gratings are fabricated accurately and efficiently. In the present study, three types of LC gratings, which hereafter referred to as the “continuous,” “binary,” and “planar TN,” are fabricated. These LC gratings are fabricated using the common two-beam interference optical

system shown in **Figure 5**. The light source was He-Cd laser which was the same as that used in the previous experiment of the one-step photoalignment. The cross-sectional area of the beam was expanded to 0.04 cm^2 . The crossing angle was 0.3° , and the resultant modulation period of the electric field was $60 \text{ }\mu\text{m}$. The polarization states of the interfering beams were adjusted using the half-/quarter-wave plates. The intensity ratio of the interfering beams can be controlled by adjusting the polarization azimuth, which was an incident on the polarization beam splitter, using the half-wave plate. The one-step holographic photoalignment for the fabrication of the three types of LC gratings is described below individually. The empty glass cells used in the present experiment were the same as that described in Section 2.2. Moreover, the annealing process after the UV exposure and the injection process of nematic LCs were also the same.

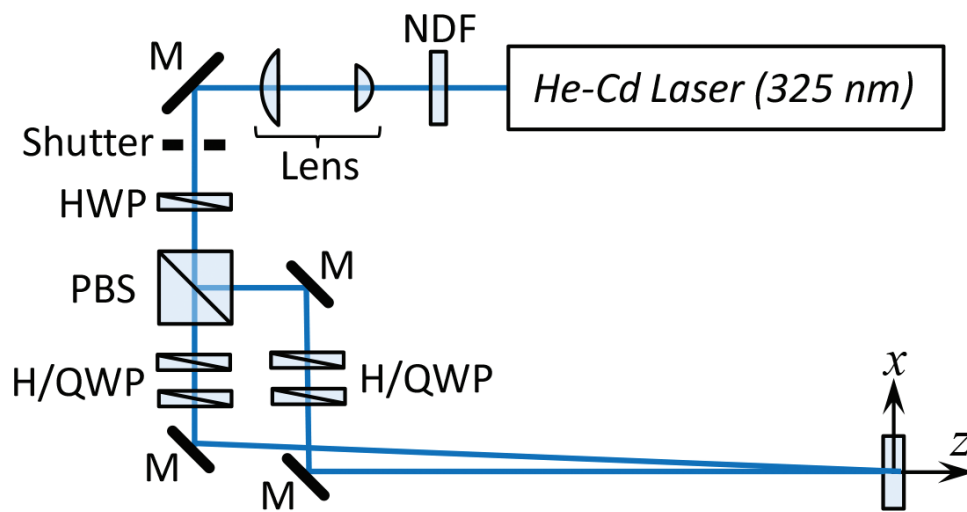


Figure 5. Optical system for two-beam interference exposure. NDF, M, PBS, and H/QWP represent the neutral-density filter, mirror, polarization beam splitter, and half-/quarter-wave plates.

3.1.1. Continuous LC gratings

Figure 6 shows the fabrication procedure for the continuous LC grating with 0° planar or with 90° TN alignment. In the continuous LC grating, LC directors are constantly rotated along the grating vector. These were fabricated by one-step circular polarization interference exposure. When two orthogonally circular polarized beams interfere with each other, the polarization azimuth of the linear polarization in the interference field is continuously modulated; however, the polarization ellipticity and the intensity are not modulated. Therefore, the periodic alignment process, in which alignment directions are continuously rotated along the grating vector, can be simultaneously applied to two P6CB alignment films in the empty glass cell. Moreover, the same alignment pattern and the orthogonal pattern with each other (i.e., the period of the pattern is shifted by a half period with each other) can be applied into the empty glass cell by adjusting the exposure dose as shown in **Figure 6(b)**. In this experiment, the beam powers of both interfering two beams were set to 2 mW . The exposure doses to fabricate the

continuous LC grating with planar and with TN alignment were set to 400 mJ/cm^2 and 200 mJ/cm^2 , and the exposure times were set to 8.0 s and 4.0 s, respectively. The self-diffraction from the front P6CB substrate during the photoalignment process does not occur because the optical anisotropy of P6CB is induced after annealing. The continuous LC gratings with planar or with TN alignment were fabricated by injecting the nematic LC after annealing process as shown in **Figure 6(c)**.

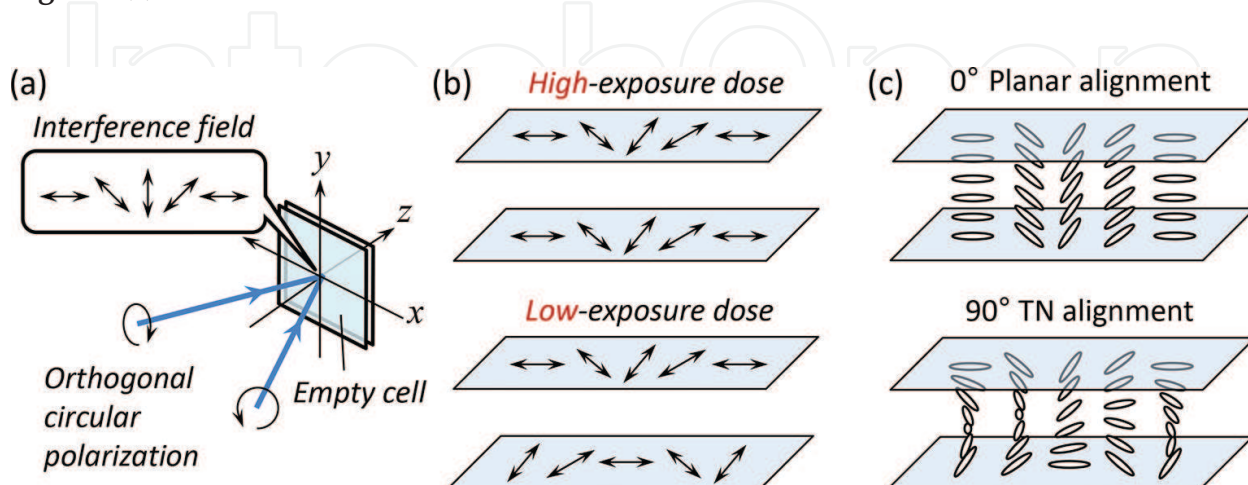


Figure 6. Schematic of the fabrication procedure for the continuous LC grating. (a) One-step exposure of an empty glass cell to a UV interference beam obtained by interfering reverse rotated circularly polarized beams with each other, (b) periodic alignment patterns after annealing in the P6CB films, and (c) director distributions after injecting with a nematic LC (5CB).

3.1.2. Binary LC gratings

Figure 7 shows the fabrication procedure for the binary LC grating with 0° planar or with 90° TN alignment. In the binary LC grating, LC directors are changed periodically and discretely by 90° in the grating vector. These were fabricated by one-step exposure of the empty glass cells to the UV interference field obtained by the interference of linearly polarized beams which were inclined $+45^\circ$ and -45° from the x -axis. The interference field periodically modulates the polarization states only because the $+45^\circ$ and -45° linear polarizations are orthogonality relation. The polarization ellipticity in the interference field is continuously modulated in the range from 0.0 to 1.0, and the polarization azimuth is discretely changed by 90° at the boundary point where the polarization ellipticity is 1.0; the polarization state changes between $\pm S_3$ via $\pm S_1$ in Poincaré sphere. Considering that the alignment direction of P6CB in the alignment films is predominantly in the longitudinal direction of the irradiated elliptical polarization, the alignment direction in the alignment films is periodically and discretely changed by 90° after annealing as shown in **Figure 7(b)**. However, the regions in the alignment films which were irradiated elliptical or circular polarization involve the decline in the anchoring energy. In this experiment, the exposure doses to fabricate the continuous grating with planar and with TN alignment were set to 600 mJ/cm^2 and 200 mJ/cm^2 . Other experimental conditions and fabrication procedure were identical to those for the previously described continuous LC gratings.

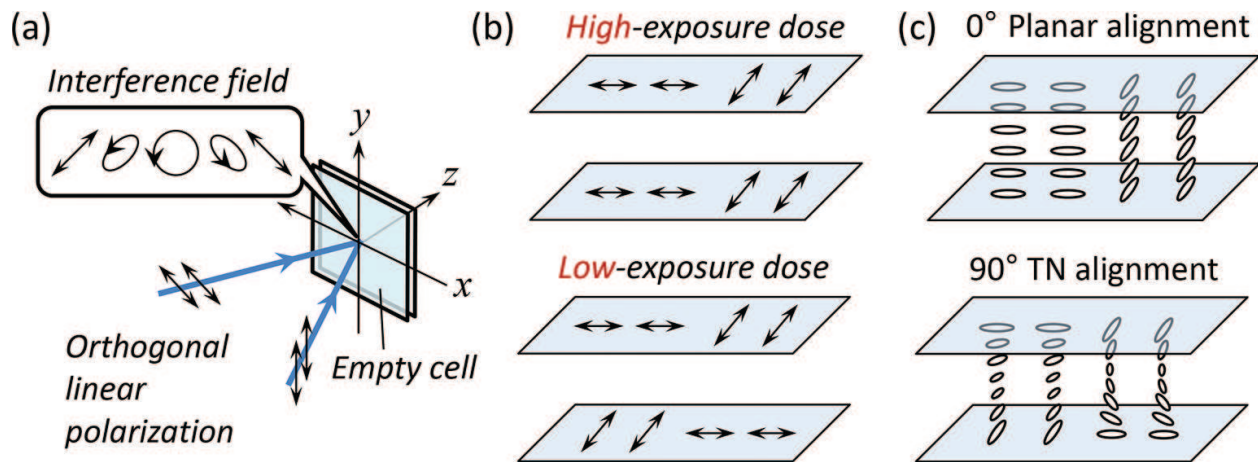


Figure 7. Schematic of the fabrication procedure for the binary LC grating. (a) One-step exposure of an empty glass cell to a UV interference beam obtained by interfering orthogonal linearly polarized beams with each other, (b) periodic alignment patterns after annealing in the P6CB films, and (c) director distributions after injecting with a nematic LC (5CB).

3.1.3. Planar-TN-LC grating

Figure 8 shows the fabrication procedure for the planar-TN-LC grating. In the planar-TN-LC grating, 0° planar and 90° TN alignment are periodically intermixed in the grating vector. This was fabricated by one-step exposure of the empty glass cell to the UV interference field obtained by the interference of linearly polarized beams which were inclined 90° from the x -axis. The interference field periodically modulates the intensity only. When the beam powers of interfering two beams are the same, the visibility of the interference field is maximum. This indicates that there are regions where the intensity in the interference field is nearly zero; the photoalignment is not applied in these regions. Therefore, the beam power ratio of the interfering linearly polarized beams was intentionally shifted from 1:1 to reduce the visibility from 1.0. Moreover, the planar-TN-LC grating can be fabricated by adjusting to the appropriate beam power ratio because the exposure dose varies along the x -axis position. The maximum intensity I_{\max} and minimum intensity I_{\min} in the interference field can be calculated as

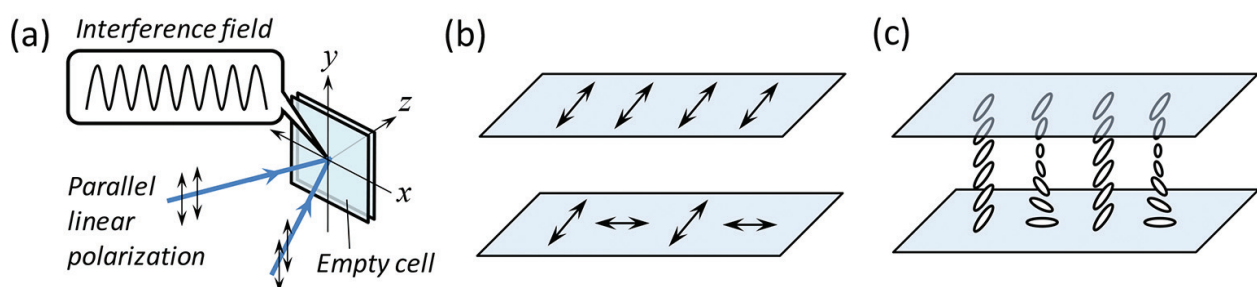


Figure 8. Schematic of the fabrication procedure for the planar-TN-LC grating. (a) One-step exposure of an empty glass cell to a UV interference beam obtained by interfering parallel linearly polarized beams with each other, (b) periodic alignment patterns after annealing in the P6CB films, and (c) director distributions after injecting with a nematic LC (5CB).

$$\begin{cases} I_{\max} = I_1 + I_2 + 2\sqrt{I_1 I_2}, \\ I_{\min} = I_1 + I_2 - 2\sqrt{I_1 I_2}, \end{cases} \quad (1)$$

where I_1 and I_2 represent the beam intensities of the interfering beams. As calculation conditions, $I_{\max} = 600 \text{ mJ/cm}^2$ and $I_{\min} = 200 \text{ mJ/cm}^2$ were set. From these conditions, I_1 and I_2 were determined to be 2.5 mW/cm^2 and 37.5 mW/cm^2 , and the derived exposure time is 10 s. However, in the result of the preliminary experiment based on this condition, planar areas were larger than the TN areas in the resultant planar-TN-LC grating (i.e., an overall ratio of the planar and the TN areas was not 1:1). Therefore, the exposure time was experimentally determined in 8.0 s to achieve an overall 1:1 ratio of the planar and the TN areas. Other experimental conditions and fabrication procedure were identical to those for the previously described continuous LC gratings.

3.2. Observation results of director distributions by polarized light microscopy

Figure 9(a) and **(b)** shows the photographs of the continuous LC grating with planar and with TN alignment, respectively. The transmittance in the photographs continuously varies along the grating vector. The full dark fields, where the LC directors incline by 0° or 90° with respect to the transmission axes of the polarizer and the analyzer, exist in the planar alignment of the continuous LC grating as shown in **Figure 9(a)**. Note that the transmittance of the bright fields, where the LC directors incline by 45° with respect to the transmission axes, depends on the retardation of the LC grating. This is because the polarization state of output electric field changes between $\pm S_3$ in Poincaré sphere depending on the retardation when the linear polarization inclined by 45° with respect to an optical axis is incident. In the TN alignment shown in **Figure 9(b)**, when the LC directors of the alignment film interface incline by 0° or 90° with transmission axes of the polarizer and the analyzer, the transmittance of white light is maximized. Full dark fields do not exist. **Figure 9(c)** and **(d)** shows the photographs of the binary LC grating with planar and with TN alignment, respectively. For the reasons described above, the entire region can be seen as full dark fields in the planar alignment as shown in **Figure 9(c)**, and the entire region can be seen as bright fields in the TN alignment as shown in **Figure 9(d)**. Moreover, vertical lines extending perpendicular to the grating vector direction are observed. These lines represent the “transition regions” between the binary regions, which will be detailed later. **Figure 9(e)** shows the photographs of the planar-TN-LC grating. The full dark fields and the bright fields are seen to alternate, and the distribution of full dark fields and bright fields is inverted by interchanging the crossed Nicol and parallel Nicol polarizers, as shown in **Figure 9(e-1)** and **(e-2)**. These results indicated that the director distributions of the resultant LC gratings were nearly the same as the initially designed director distributions shown in **Figures 6(c)**, **7(c)**, and **8(c)**.

3.3. Numerical analysis of director distributions and diffraction properties

It is important to consider quantitatively the observed director distributions of the resultant LC gratings based on a physical theory. The director distributions of the LC gratings are not determined uniquely and strictly by only patterns of alignment films. Therefore, in some case, the slightly different director distributions from the ideal distributions were obtained as

described in Section 3.2. In this section, the estimation method of the static director distributions based on the elastic continuum theory of a nematic LCs is described below.

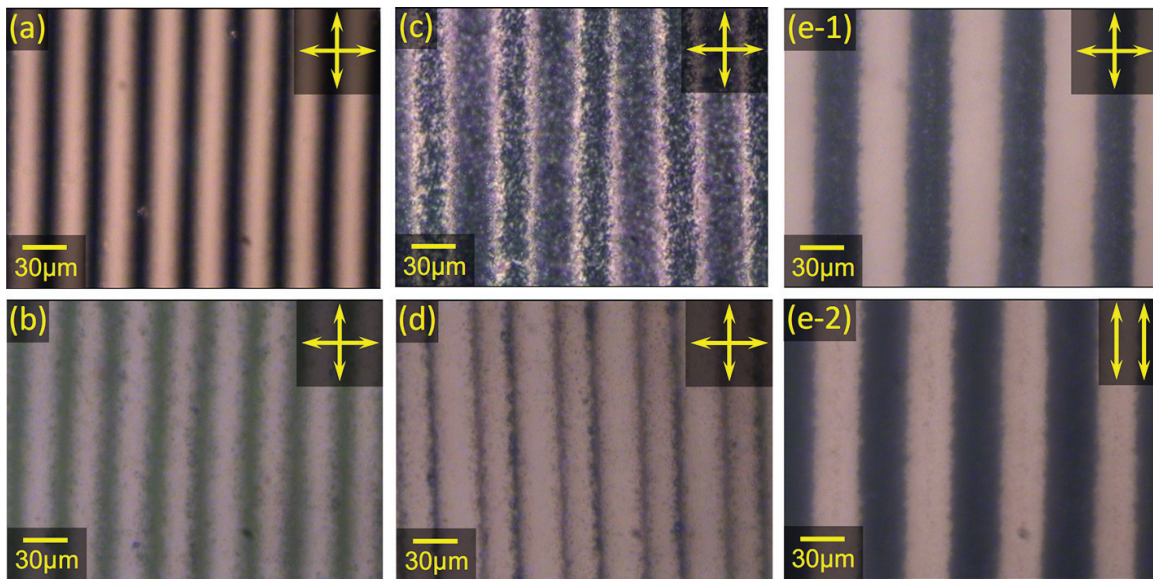


Figure 9. Photographs of the resultant LC gratings observed by polarized light microscopy. (a) Continuous LC gratings with planar alignment and (b) TN alignment. (c) Binary LC gratings with planar alignment and (d) TN alignment. (e) Planar-TN-LC gratings under (e-1) crossed Nicol polarizers and (e-2) parallel Nicol polarizers. The part of the figure is reproduced by the kind permission of *The Optical Society of America* from *Applied Optics* 54, 6010-6018 (2015).

In LC gratings, LCs are anchored by alignment films, and then spatial nonuniformities in LC directors are induced. Since LCs have elastic properties, restoring forces and elastic free energies are increased by these elastic deformations. Moreover, when the spatial nonuniformities (i.e., total elastic free energies) are minimized, the periodic director distributions of the LC gratings are stable. Therefore, the detailed director distributions can be estimated by calculating the condition which the total free energy is minimized. The total elastic free energy of the LC grating is obtained by spatially integrating the elastic free energy per unit volume shown in the following equation:

$$f = \frac{1}{2}K_1(\nabla \cdot \mathbf{n})^2 + \frac{1}{2}K_2[\mathbf{n} \cdot (\nabla \times \mathbf{n})]^2 + \frac{1}{2}K_3|\mathbf{n} \times (\nabla \times \mathbf{n})|^2, \quad (2)$$

where K_1 , K_2 , and K_3 represent the elastic constants the splay, twist, and bend of nematic LCs, respectively. \mathbf{n} represents the director of the nematic LCs in the xyz coordinate frame. The x -axis is parallel to the grating vector, and the z -axis is parallel to the thickness direction which follows to the definition shown in Section 3.1. Based on the premise that the director is not tilted in the z -axis, the director \mathbf{n} is defined as $\mathbf{n} = (\cos\phi, \sin\phi, 0)$, where ϕ represents the angle between the x -axis and the director \mathbf{n} . By substituting the director \mathbf{n} into Eq. (2), we obtain

$$f = \frac{1}{2}K_1 \left(\frac{\partial\phi}{\partial x} \right)^2 \sin^2\phi + \frac{1}{2}K_2 \left(\frac{\partial\phi}{\partial z} \right)^2 + \frac{1}{2}K_3 \left(\frac{\partial\phi}{\partial x} \right)^2 \cos^2\phi, \quad (3)$$

where $K_1 = 6.4$ pN, $K_2 = 3.0$ pN, and $K_3 = 10.0$ pN [12]. The total elastic free energy F of one period is obtained by spatially integrating Eq. (3) as given by

$$F = \int_0^d \int_0^\Lambda f dx dz, \tag{4}$$

where d and Λ represent the cell gap and the grating pitch of LC gratings, respectively. As described above, the director distribution is determined by calculating ϕ when the total elastic free energy is minimized. Specifically, the director distribution can be calculated as $\partial F = 0$. We adopted the finite element method to solve this variational problem of the functional. In this numerical calculation, we applied periodic boundary conditions for speeding up the calculation. Moreover, we set fixed boundary conditions in the alignment substrates at $z = 0$ and $z = d$ by assuming strong anchoring conditions of P6CB alignment films shown in **Table 1**.

Boundary position	Continuous		Binary		Planar-TN
	Planar	TN	Planar	TN	
$z = 0$	$\pi x/\Lambda$	$\pi x/\Lambda$	$0(0 \leq x < \Lambda/2)\pi/2$ $(\Lambda/2 \leq x \leq \Lambda)$	$0(0 \leq x < \Lambda/2)\pi/2$ $(\Lambda/2 \leq x \leq \Lambda)$	$\pi/2$
$z = d$	$\pi x/\Lambda$	$\pi x/\Lambda + \pi/2$	$0(0 \leq x < \Lambda/2)\pi/2(\Lambda/2 \leq x \leq \Lambda)$	$\pi/2(0 \leq x < \Lambda/2)0$ $(\Lambda/2 \leq x \leq \Lambda)$	$0(0 \leq x < \Lambda/2)\pi/2$ $(\Lambda/2 \leq x \leq \Lambda)$

Table 1. Boundary conditions of the three types of LC gratings $\phi(x)$ at $z = 0$ and $z = d$.

Figure 10 shows a cross-sectional view of the director distributions in the LC gratings over one period as calculated by the elastic continuum theory of nematic LCs. The ideal director distributions shown in Section 3.1 were obtained. However, especially in the binary LC gratings [**Figure 10(c)** and **(d)**], the LC directors do not change abruptly at the boundary of two regions (i.e., previously described “transition regions”). These results indicate that LC directors in the LC grating are not induced steep elastic deformations in order to prevent increasing locally elastic free energies.

To consider quantitatively the effects on the diffraction properties due to transition regions, the numerical solutions of the diffraction properties are calculated on the basis of Jones calculus using the obtained director distribution shown in **Figure 10**. To calculate the phase distributions of the nematic LC phases, we consider the birefringence plate of n layers, and the Jones matrix \mathbf{W} of the LC gratings can be written as

$$\mathbf{W}(x) = \mathbf{W}_{\text{out}}(x) \cdot \left(\prod_{m=1}^n \mathbf{W}_m(x) \right) \cdot \mathbf{W}_{\text{in}}(x), \tag{5}$$

where \mathbf{W}_{in} and \mathbf{W}_{out} are Jones matrices for the P6CB alignment films at the input and output sides, respectively, and \mathbf{W}_m represents the LC phase of the m th layer. These are given by

$$\mathbf{W}_{\text{in/out}}(x) = \mathbf{R}[-\phi(x)] \cdot \begin{bmatrix} \exp(-i\pi\Delta n_P d_P/\lambda) & 0 \\ 0 & \exp(i\pi\Delta n_P d_P/\lambda) \end{bmatrix} \cdot \mathbf{R}[\phi(x)], \quad (6)$$

$$\mathbf{W}_m(x) = \mathbf{R}[-\phi(x)] \cdot \begin{bmatrix} \exp(-i\pi\Delta n d_m/\lambda) & 0 \\ 0 & \exp(i\pi\Delta n d_m/\lambda) \end{bmatrix} \cdot \mathbf{R}[\phi(x)], \quad (7)$$

where \mathbf{R} represents the coordinate rotation matrix. Δn and Δn_P are the optical anisotropy of the nematic LCs and the P6CB alignment films, respectively. λ is the wavelength of the probe beam. d_m and d_P represent the thicknesses of the nematic LC layers ($d/n = d_m$) and P6CB alignment films, respectively. The parameters used in the calculation are $\Delta n = 0.18$, $\Delta n_P = 0.2$, $d_P = 300$ nm, and $\lambda = 633$ nm. The electric field transmitted through the LC gratings is obtained by multiplying the incident electric field vector by the Jones matrices \mathbf{W} . The diffraction properties are obtained by Fourier transform of the spatial distributions of the output electric field vector. The resultant numerical solutions of the diffraction properties will be described later in conjunction with the measurement results.

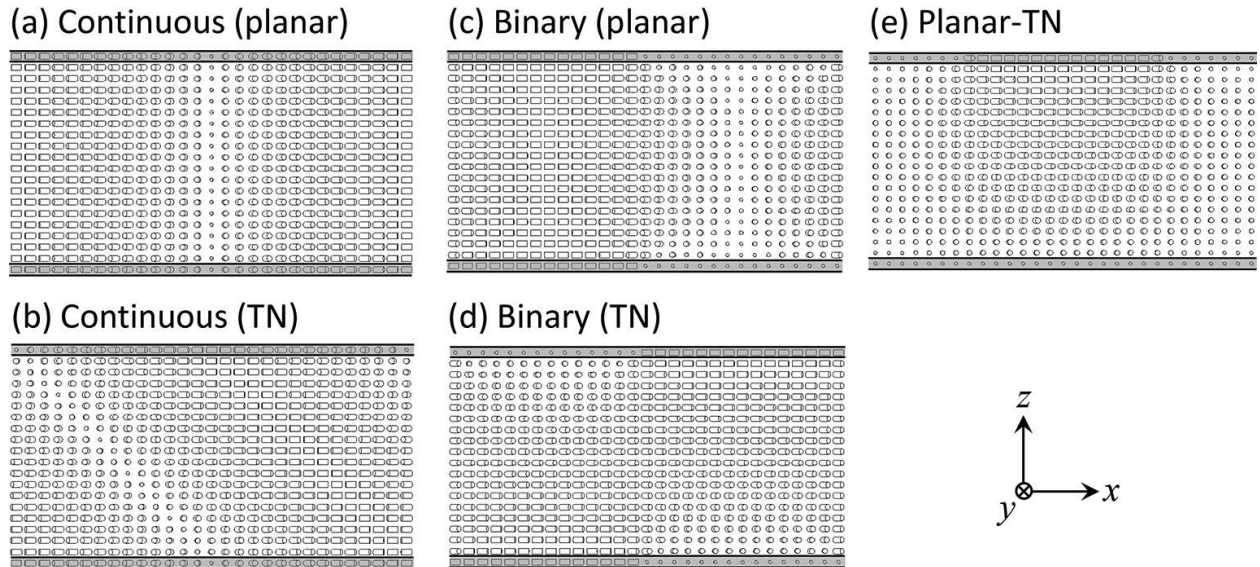


Figure 10. Cross-sectional view of the director distributions calculated from the elastic continuum theory. (a) Continuous LC gratings with planar alignment and (b) TN alignment. (c) Binary LC gratings with planar alignment and (d) TN alignment. (e) Planar-TN-LC gratings. Fixed boundary conditions shown in **Table 1** are applied in gray regions. The part of the figure is reproduced by the kind permission of *The Optical Society of America* from *Applied Optics* 54, 6010-6018 (2015).

3.4. Analytical solutions by Jones calculus

It is important to obtain mathematically the analytical solutions of diffraction properties to give exact theoretical solutions. In this section, the analytical solutions of the resultant LC gratings are derived using Jones calculus. However, the transition regions are not considered in this analysis, and the ideal director distributions shown in Section 3.1 are analyzed. Comparisons of the analytical solutions and the numerical solutions will be described in Section 3.5. The variables which are defined in the previous section are taken over.

3.4.1. Continuous LC gratings

In the resultant continuous LC gratings, the alignment direction of the 0° planar alignment or 90° TN alignment is rotated continuously along the grating vector [Figure 6(a)]. Therefore, rotation matrix which depends on the position ξ ($=2\pi x/\Lambda$) in the grating vector is introduced into the Jones matrix of the continuous LC gratings as shown in the following:

$$\mathbf{W}_{\text{planar/TN}}^{\text{continuous}} = \mathbf{R}\left(-\frac{\xi}{2}\right) \cdot \mathbf{W}_{\text{Planar/TN}} \cdot \mathbf{R}\left(\frac{\xi}{2}\right), \quad (8)$$

where $\mathbf{W}_{\text{Planar}}$ and \mathbf{W}_{TN} represent Jones matrices of the 0° planar and 90° TN alignment, respectively, as shown in the following:

$$\mathbf{W}_{\text{planar}} = \begin{bmatrix} \exp(-i\frac{\Gamma}{2}) & 0 \\ 0 & \exp(i\frac{\Gamma}{2}) \end{bmatrix}, \quad (9)$$

$$\mathbf{W}_{\text{TN}} = \mathbf{R}(-\Phi) \cdot \begin{bmatrix} \cos X - i\frac{\Gamma \sin X}{2X} & \Phi \frac{\sin X}{X} \\ -\Phi \frac{\sin X}{X} & \cos X + i\frac{\Gamma \sin X}{2X} \end{bmatrix}, \quad (10)$$

where Γ ($=2\pi\Delta nd/\lambda$) stands for the phase retardation, Φ ($=\pi/2$) represents the twisted angle in the TN alignment, and X is defined as $\sqrt{\Phi^2 + (\Gamma/2)^2}$. By substituting the Eq. (9) or (10) into Eq. (8) and separating perturbation terms which depend on the position ξ , we obtain the Jones matrices of the continuous LC gratings with the planar or with TN alignment which contribute to ± 1 st-order diffraction, as follows:

$$\mathbf{W}_{\text{planar}}^{\text{continuous}} = \frac{i}{2} \sin \frac{\Gamma}{2} \begin{bmatrix} 1 & \pm i \\ \pm i & -1 \end{bmatrix} \exp(\pm i\xi), \quad (11)$$

and

$$\mathbf{W}_{\text{TN}}^{\text{continuous}} = i \frac{\Gamma \sin X}{4X} \begin{bmatrix} \mp i & -1 \\ -1 & \pm i \end{bmatrix} \exp(\pm i\xi) \quad (12)$$

The electric field vector of the ± 1 st-order diffracted beam is derived by multiplying the electric field vector of the incident beam shown in the following:

$$\mathbf{E}_{\text{in}} = \begin{bmatrix} (\cos \Psi) \exp(i\delta) \\ \sin \Psi \end{bmatrix}, \quad (13)$$

where Ψ and δ represent the amplitude ratio angle and the phase difference. Therefore, the electric field vector of the ± 1 st-order diffracted beams are given by

$$\mathbf{E}_{\text{out (planar)}} = \mathbf{W}_{\text{planar}}^{\text{continuous}} \cdot \mathbf{E}_{\text{in}} = \frac{i}{2} \sin \left(\frac{\Gamma}{2}\right) \exp(\pm i\xi) \cdot \{ \cos \Psi \exp(i\delta) \pm i \sin \Psi \} \begin{bmatrix} 1 \\ \pm i \end{bmatrix}, \quad (14)$$

and

$$\mathbf{E}_{\text{out (TN)}} = \mathbf{W}_{\text{TN}}^{\text{continuous}} \cdot \mathbf{E}_{\text{in}} = i \frac{\Gamma \sin X}{4X} \exp(\pm i\xi) \cdot \{\mp i \cos \Psi \exp(i\delta) - \sin \Psi\} \begin{bmatrix} 1 \\ \mp i \end{bmatrix}. \quad (15)$$

These analytical solutions indicate that the polarization states of the ± 1 st-order diffracted beams from both the planar and the TN alignment are always circular polarization, and this property does not depend on the polarization states of the incident beams. Either of +first- or –first-order diffraction beam only diffracts when the circular polarization is incident (i.e., $\delta = \pi/2$, and $\Psi = \pi/4$); both +first- and –first-order diffraction beams diffract when the linear polarization is incident (i.e., $\delta = 0$). In the case of the entering the circular polarization, the diffraction efficiency is twice in comparison with the diffraction efficiency when the linear polarization is incident; these are obtained by squaring the electric field of the ± 1 st-order diffracted beams shown in Eqs. (14) and (15).

3.4.2. Binary LC gratings and planar-TN grating

Both the binary and the planar-TN-LC gratings are classified into the diffraction gratings in which the amount of the phase shift is rectangularly modulated along the grating vector. The diffraction properties of thin anisotropic diffraction gratings, in which two different anisotropic regions are periodically arranged, can also be analyzed by Jones calculus [12]. Diffraction properties of the binary LC gratings and the planar-TN-LC grating are given by the sum of the emitted electric fields from the two anisotropic regions. Therefore, the Jones matrix \mathbf{W}_N of the N th-order diffracted beam is given by Fourier transform when the Jones matrices of the two anisotropic regions are defined as \mathbf{W}_A and \mathbf{W}_B and can be written as

$$\mathbf{W}_N = \frac{1}{\Lambda} \left[\int_{-\Lambda/2}^{\zeta\Lambda} \mathbf{W}_A \exp\left(-i \frac{2\pi x N}{\Lambda}\right) dx + \int_{\zeta\Lambda}^{\Lambda/2} \mathbf{W}_B \exp\left(-i \frac{2\pi x N}{\Lambda}\right) dx \right], \quad (16)$$

where ζ is the boundary position of the two anisotropic regions and defined as ($-1/2 \leq \zeta \leq 1/2$). Note that the Jones matrices \mathbf{W}_A and \mathbf{W}_B are not dependent on the x position in the integration interval. The Jones matrix \mathbf{W} is given by

$$\mathbf{W}_N = \exp\left[-i\pi N \left(\zeta - \frac{1}{2}\right)\right] \frac{\sin\left[\pi N \left(\zeta + \frac{1}{2}\right)\right]}{\pi N} (\mathbf{W}_A - \mathbf{W}_B). \quad (17)$$

Eq. (17) can also be applied to any grating when \mathbf{W}_A and \mathbf{W}_B in an anisotropic diffraction grating are known. Moreover, when the area ratio of the two anisotropic regions of \mathbf{W}_A and \mathbf{W}_B is 1:1 (i. e., $\zeta = 0$), even-order diffracted beams are not diffracted as shown in Eq. (17). This is because the even-order diffracted beams are negated by the anti-phase emitted electric field.

To derive the Jones matrices of the binary LC grating with 0° planar and with 90° TN alignments, \mathbf{W}_A are defined by the right-hand side of the Eqs. (9) and (10) described in the previous section, respectively. On the other hand, the alignment directions of \mathbf{W}_B are inclined by 90° with the alignment directions of \mathbf{W}_A , and \mathbf{W}_B are given by

$$\mathbf{W}_B = \mathbf{R}\left(-\frac{\pi}{2}\right) \cdot \mathbf{W}_A \cdot \mathbf{R}\left(\frac{\pi}{2}\right). \quad (18)$$

The Jones matrices of the ± 1 st-order diffraction from the binary LC grating with 0° planar and with 90° TN alignments are given by substituting the Jones matrices described in Eqs. (9) or (10) and (18) into Eq. (17) and can be written as

$$\mathbf{W}_{\text{planar}}^{\text{binary}} = \frac{2}{\pi} \sin \frac{\Gamma}{2} \begin{bmatrix} 1 & 0 \\ 0 & -1 \end{bmatrix}, \quad (19)$$

and

$$\mathbf{W}_{\text{TN}}^{\text{binary}} = \frac{\Gamma \sin X}{2\pi X} \begin{bmatrix} 0 & 1 \\ 1 & 0 \end{bmatrix}. \quad (20)$$

The Jones vectors for ± 1 st-order diffraction is derived by multiplying the electric field vector of the incident beam shown in Eq. (13) and can be written as

$$\mathbf{E}_{\text{out (planar)}} = \mathbf{W}_{\text{planar}}^{\text{binary}} \cdot \mathbf{E}_{\text{in}} = \frac{2}{\pi} \sin \frac{\Gamma}{2} \begin{bmatrix} (\cos \Psi) \exp(i\delta) \\ -\sin \Psi \end{bmatrix}, \quad (21)$$

and

$$\mathbf{E}_{\text{out (TN)}} = \mathbf{W}_{\text{TN}}^{\text{binary}} \cdot \mathbf{E}_{\text{in}} = \frac{\Gamma \sin X}{2\pi X} \begin{bmatrix} \sin \Psi \\ (\cos \Psi) \exp(i\delta) \end{bmatrix}, \quad (22)$$

The sign of the y component in Jones vector for the planar alignment shown in Eq. (21) is different than the Jones vector of the probe beam. On the other hand, the Jones vector for the TN alignment shown in Eq. (22) is the same as the probe beam Jones vector where the x and y components are interchanged. These results indicate that the binary gratings have diffraction properties which convert the polarization azimuth and the rotational direction of the polarized probe beam.

In the planar-TN-LC grating, \mathbf{W}_A and \mathbf{W}_B in the Eq. (17) are given by Eqs. (9) and (10), respectively. In the same way, the Jones vector for the ± 1 st-order diffraction from the planar-TN-LC grating is given by

$$\mathbf{E}_{\text{out(planar-TN)}} = \mathbf{W}^{\text{planar-TN}} \cdot \mathbf{E}_{\text{in}} = \frac{i}{\pi} \cdot \begin{bmatrix} \frac{\pi \sin X}{2X} - \exp(-i\frac{\Gamma}{2}) & -\cos X - i\frac{\Gamma \sin X}{2X} \\ \cos X - i\frac{\Gamma \sin X}{2X} & \frac{\pi \sin X}{2X} - \exp(i\frac{\Gamma}{2}) \end{bmatrix} \cdot \begin{bmatrix} (\cos \Psi) \exp(i\delta) \\ \sin \Psi \end{bmatrix}. \quad (23)$$

In the planar-TN-LC gratings, analytical solutions of the diffraction properties cannot be derived unconditionally because the diffraction properties depend on the phase retardation Γ , as shown in Eq. (23). The diffraction properties can be analyzed by fitting to the experimental results using the phase difference (especially the cell gap, d) as a fitting parameter.

3.5. Measurement results of diffraction properties

The \pm first-order diffracted beams from the resultant LC gratings were probed experimentally with He-Ne laser beam with a wavelength of 633 nm. The polarization states of the probe beam were adjusted to a linear or a circular polarization using a half-wave plate and a quarter-wave plate. The polarization azimuth of the probe beam was defined as the inclination angle of the polarization director with respect to the grating vector. The probe beam was incident normal to the plane of the substrate including the grating vector. The \pm first-order diffracted beams were separated from other orders using a pinhole. The diffracted beam intensities were measured using an optical power meter. The polarization states of diffracted beams were measured by a rotating analyzer method using a Glan-Thompson prism as the analyzer.

Figure 11(a) shows the measurement and the calculation results of polarization states of the \pm first-order diffracted beams from the continuous LC gratings. The calculated results are obtained from the numerical solutions described in Section 3.3 and the analytical solutions described in Section 3.4. The calculated diffraction efficiencies were fitted to the experimental results using the cell gaps as the fitting parameter, and the optimum cell gaps in the planar and TN alignment obtained by fitting were 13.2 μm and 13.1 μm , respectively. The polarization states of the \pm first-order diffracted beams from both the planar and the TN alignments are always circular polarization, and this property does not depend on the polarization states of the incident beams. Either of +first- or –first-order diffraction beam only diffracts when the circular polarization is incident; both +first- and –first-order diffraction beams diffract when the linear polarization is incident. The diffraction efficiency when the circular polarization is incident is twice in comparison with the diffraction efficiency when the linear polarization is incident.

Figure 11(b) shows the measurement and the calculation results of polarization states of the \pm 1st-order diffracted beams from the binary LC gratings. The polarization ellipticity of the diffracted beam is conserved from the probe beam, although the rotation direction is inverted from the probe beam. The polarization azimuth of the diffracted beam varies over a range from 0° to 90° depending on the polarization azimuth of the probe beam. Furthermore, the polarization azimuth of the diffracted beams is 90° offset from the planar and TN alignment when the probe beam is linearly polarized. The diffraction properties in the positive and negative diffraction orders were the same. The polarization states of the diffracted beam do not depend on the phase difference. The calculated diffraction efficiencies were fitted to the experimental results using the cell gaps as the fitting parameter, and the optimum cell gaps in both the planar and TN alignments obtained by fitting were 13.4 μm . There were slight differences in some results between the experimental results and the calculation results. These discrepancies can be mainly attributed to the transition regions at the boundary of the two alignment regions. In the calculated results, there were only slightly differences between the analytical and numerical solutions because the transition regions were considered in the numerical solutions. Specifically, with circular polarization of the probe beam, the polarization ellipticity of the diffracted beams determined with the analytical solution was 1.0; the numerical solution yielded 0.97. From that above, the cause of the slight deviation between the experimental results and the theoretical expectations is that the transition distributions in the resultant binary LC gratings were slightly larger than the estimated director distributions.

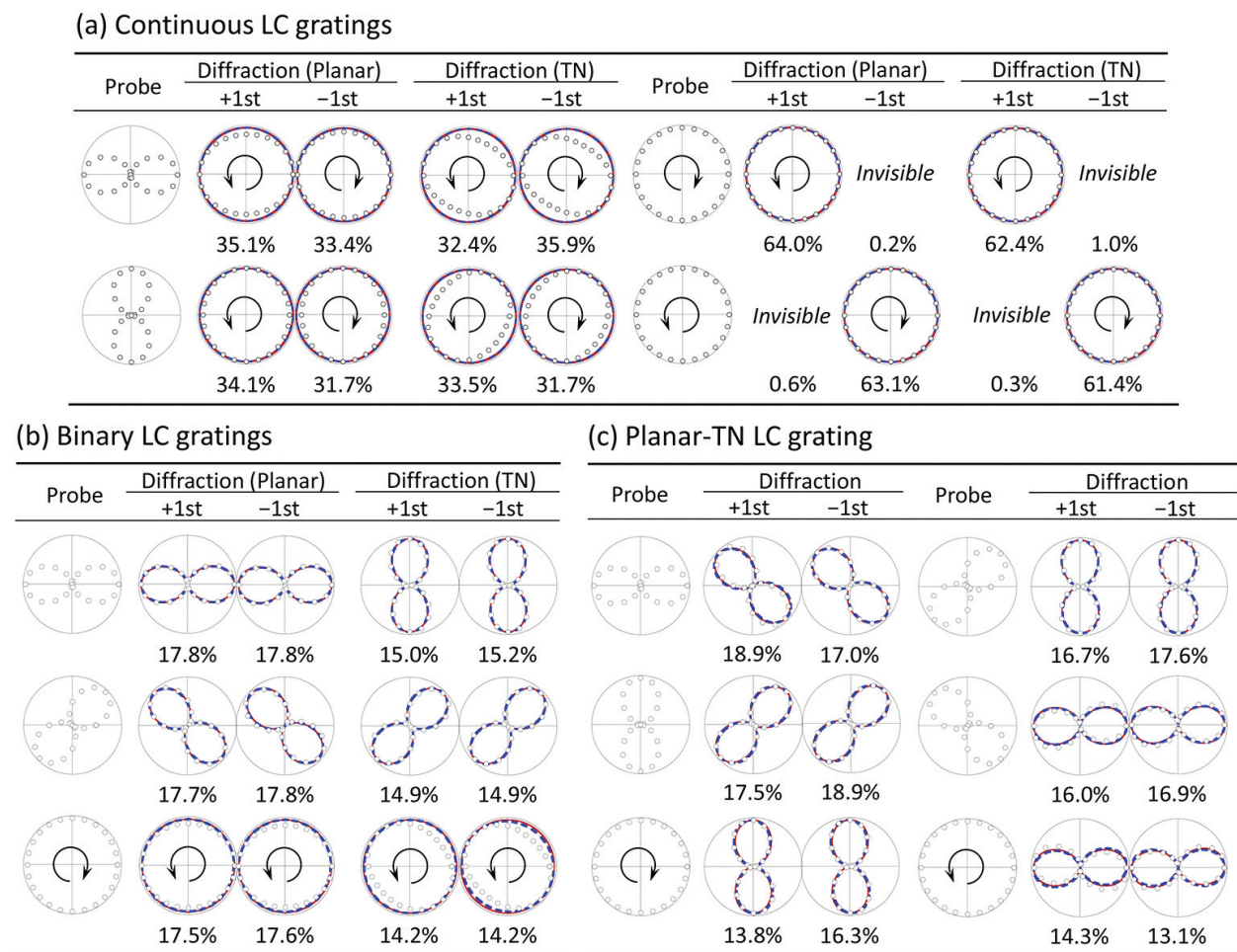


Figure 11. Polar plots of the ± 1 st-order diffracted beam for the resultant LC gratings. Open circles, red solid curves, and blue broken lines represent the experimental data, theoretical solution, and numerical solution, respectively. The numerical values below the polar plots represent the experimental results of diffraction efficiency. (a) Continuous LC gratings and (b) binary LC gratings with planar alignment and with TN alignment. (c) Planar-TN-LC gratings. The part of the figure is reproduced by the kind permission of *The Optical Society of America* from *Applied Optics* 54, 6010-6018 (2015).

Figure 11(c) shows the measured and the calculated results of the planar-TN-LC grating. There is good agreement between the measured results and the analytical and numerical solutions. When the probe beam was right- and left-hand circularly polarized, the elliptically polarized beams, with polarization azimuths offset by 90° , were diffracted depending on the rotation direction of the probe beams. The polarization azimuth of both probe beam and the diffracted beam is inversely related. The polarization ellipticity of the diffracted beams periodically varies over the range of 0.0–0.2 depending on the polarization azimuth of the probe beam. When the probe beams were 0° and 90° linearly polarized, the polarization ellipticity of diffracted beams was 0.0. On the other hand, when the probe beams were $\pm 45^\circ$ linearly polarized, the ellipticity was 0.2. It was found from the theoretical analysis that the polarization ellipticity of the diffracted beam varies over the 0.0–0.9 range, depending on the phase difference when the probe beam was $\pm 45^\circ$ linearly polarized. In addition, when the probe beams are 0° and 90° linearly polarized, the diffracted beams are always linearly polarized and do not depend on the phase difference. The calculated diffraction properties were fitted to the experimental results using the cell gap as the

fitting parameter, and the optimum cell gap in the planar-TN-LC grating obtained by fitting was 14.8 μm . The diffraction properties in the positive and negative diffraction orders were the same.

4. Conclusions

We demonstrated the efficient yet practical method for fabricating the LC gratings containing a TN alignment using one-step polarization holographic photoalignment. In addition, the director distributions of the resultant LC gratings are analyzed based on the elastic continuum theory and observed experimentally using a polarized light optical microscope. Furthermore, the polarization diffraction properties were measured experimentally by the incident of a visible laser and analyzed theoretically by Jones calculation. This study is of significance in that the various LC gratings containing TN alignments can be fabricated by simultaneous exposure of two P6CB substrates to the polarization interference beams. In the resultant continuous gratings, the polarization conversion properties to the circular polarization and the dependence of the propagation direction on the polarization states of the probe beams are obtained. In the resultant binary LC grating, the polarization azimuth of the diffracted beam changed ranging from 0° to 90° depending on the polarization azimuth of the probe beam. Moreover, when the probe beam is elliptical or circularly polarized, the rotation direction of the diffracted beam is converted. In the resultant planar-TN-LC grating, the polarization azimuth of both the probe beam and the diffracted beam showed an inverse relationship. In addition, the polarization ellipticity varied depending on the polarization azimuth of the probe beam. These polarization diffraction properties are well explained by theoretical analysis based on Jones calculus. These resultant LC gratings exhibit great potential for application as a diffractive optical element that can simultaneously control the various parameters of the light wave, such as amplitude, polarization states, and propagation direction.

Author details

Kotaro Kawai¹, Moritsugu Sakamoto¹, Kohei Noda¹, Tomoyuki Sasaki¹,
Nobuhiro Kawatsuki² and Hiroshi Ono^{1*}

*Address all correspondence to: onoh@nagaokaut.ac.jp

1 Department of Electrical Engineering, Nagaoka University of Technology, Nagaoka, Niigata, Japan

2 Department of Applied Chemistry, University of Hyogo, Himeji, Hyogo, Japan

References

- [1] Todorov, T., Nikolova, L., Tomova, N. Polarization holography. 2: Polarization holographic gratings in photoanisotropic materials with and without intrinsic birefringence. *Applied Optics*. 1984;23(24):4588–4591. DOI: 10.1364/AO.23.004588

- [2] Crawford, G.P., Eakin, J.N., Radcliffe, M.D., Callan-Jones, A., Pelcovits, R.A. Liquid-crystal diffraction gratings using polarization holography alignment techniques. *Journal of Applied Physics*. 2005;**98**(12):123102. DOI: 10.1063/1.2146075
- [3] Yu, C.-J., Kim, D.-W., Kim, J., Lee, S.-D. Polarization-invariant grating based on a photoaligned liquid crystal in an oppositely twisted binary configuration. *Optics Letters*. 2005;**30**(15):1995–1997. DOI: 10.1364/OL.30.001995
- [4] Komanduri R.K, Escuti M.J. High efficiency reflective liquid crystal polarization grating. *Applied Physics Letters*. 2009;**95**(9):091106. DOI: 10.1063/1.3197011
- [5] Honma, M., Nose, T. Highly efficient twisted nematic liquid crystal polarization gratings achieved by microrubbing. *Applied Physics Letters*. 2012;**101**(4):041107. DOI: 10.1063/1.4737945
- [6] Zhu, J.-L., Lu, J.-G., Qiang, J., Zhong E.-W, Ye Z.-C, He Z, et. al. 1D/2D switchable grating based on field-induced polymer stabilized blue phase liquid crystal. *Journal of Applied Physics*. 2012;**111**(3):033101. DOI: 10.1063/1.3680875
- [7] Kuzuwata, M., Sasaki, T., Kawatsuki, N., Ono, H. Fabrication of twisted nematic structure and vector grating cells by one-step exposure on photocrosslinkable polymer liquid crystals. *Optics Letters*. 2012;**37**(6):1115–1117. DOI: 10.1364/OL.37.001115
- [8] Kawai, K., Sasaki, T., Noda, K., Kawatsuki, N., Ono, H. Simple fabrication of liquid crystalline grating cells with homogeneous and twisted nematic structures and effects of orientational relaxation on diffraction properties. *Applied Optics*. 2014;**53**(17):3679–3686. DOI: 10.1364/AO.53.003679
- [9] Kawai, K., Sasaki, T., Noda, K., Sakamoto, M., Kawatsuki, N., Ono H. Holographic binary grating liquid crystal cells fabricated by one-step exposure of photocrosslinkable polymer liquid crystalline alignment substrates to a polarization interference ultraviolet beam. *Applied Optics*. 2015;**54**(19):6010–6018. DOI: 10.1364/AO.54.006010
- [10] Kawai, K., Sakamoto, M., Noda, K., Sasaki, T., Kawatsuki, N., Ono, H. Design and fabrication of a tunable wavelength-selective polarization grating. *Applied Optics*. 2016;**55**(26):6269–6274. DOI: 10.1364/AO.55.006269
- [11] Kawatsuki, N., Goto, K., Kawakami, T., Yamamoto, T. Reversion of alignment direction in the thermally enhanced photoorientation of photo-cross linkable polymer liquid crystal films. *Macromolecules*. 2002;**35**(3):706–713. DOI: 10.1021/ma011439u
- [12] Scharf, T. Polarized light in liquid crystals and polymers. Hoboken, New Jersey: John Wiley & Sons, Inc.; 2007. 400 p. DOI: 10.1002/047007437X

